Soft Matter

Vertically Oriented Nanoporous Block Copolymer Membranes for Separation and Filtration

Journal:	*Soft Matter*
Manuscript ID	SM-COM-03-2020-000526.R1
Article Type:	Communication
Date Submitted by the Author:	23-May-2020
Complete List of Authors:	Luo, Yan; University of Akron, Polymer Engineering Wang, Xiaoteng; University of Akron, Polymer Engineering Zhang, Ren; University of Akron, Polymer Engineering Singh, Maninderjeet; University of Houston System, Chemical and Biomolecular Engineering Ammar, Ali; University of Houston System, Chemical and Biomolecular Engineering Hassan, Mohamed; Qatar University, Center for Advanced Materials Ponnamma, Deepalekshmi; Qatar University, Center for Advanced Materials Adham, Samer; ConocoPhillips Co, Qatar Science & Technology Park Al-Maadeed, Mariam; Qatar University Karim, Alamgir; University of Houston System, Chemical and Biomolecular Engineering

Vertically Oriented Nanoporous Block Copolymer Membranes for Separation and Filtration

Yan Luo,[1] Xiaoteng Wang,[1] Ren Zhang,[1] Maninderjeet Singh,[2] Ali Ammar,[2] Mohammad K. Hassan,[3] Deepalekshmi Ponnamma, [3] Samer Adham, [4] Mariam Al Ali Al-Maadeed,[3,5] Alamgir Karim[1,2]*

[1]Department of Polymer Engineering, University of Akron, Akron, OH 44325

[2]Department of Chemical and Biomolecular Engineering, University of Houston, Houston, TX 77204

[3]Center for Advanced Materials, Qatar University, P O Box 2713, Doha, Qatar

[4]ConocoPhilips Global Water Sustainability Center, Qatar Science and Technology Park, Doha, Qatar

[5]Materials Science & Technology Program, College of Arts & Sciences, Qatar University, P O Box 2713, Doha, Qatar

Correspondence: Alamgir Karim (akarim3@Central.UH.EDU)

Abstract

The separation of oil from water and filtration of aqueous solutions and dispersions are critical issues in the processing of waste and contaminated water treatment. Membrane-based technology has been proven as an effective method for the separation of oil from water. In this research, a block copolymer (BCP) based nanoporous membrane suitable for oil/water filtration has been designed and fabricated. We used ~100 nm thick model poly(styrene-block-methymethacrylate) (PS-b-PMMA) BCP as the active top nanofiltration layer, processed using a roll-to-roll (R2R) method of cold zone annealing (CZA) to obtain vertical orientation, followed by ultraviolet (UV) irradiation selective etch of PMMA cylinders to form vertically oriented nanopores as a novel feature compared to meandering nanopores in other such systems. The cylindrical nanochannels are hydrophilic, and have a uniform pore size, narrow pore size distribution and a high pore density. The bottom supporting layer is a conventional microporous polyethersulfone (PES) membrane. The created asymmetric membrane is demonstrated to be effective for oil/water

extraction with modestly high throughput rate comparable to other RO/NF membranes. The molecular weight dependent filtration of a water soluble polymer, PEO, demonstrates the broader applications of such membranes.

Introduction

Large-scale discharge of oily contaminants in various water streams as a result of human interventions seriously impacts the living environment in an adverse fashion.[1] Recent years have witnessed numerous oil/water separation technologies capable of separating oil and water mixtures, ranging from the produced water of the petrochemical industry to the vegetable oil-contaminated municipal wastewater.[2-4] Several conventional separation techniques such as gravity separation, coagulation, air floatation, chemical and biological treatments, and use of absorbance and electric field, etc. are applied for separating oil and water mixtures. However, the operational difficulties and poor efficiency mainly leads to high cost and therefore difficult to implement.[5] Recently, membrane filtration has been proved to be one of the best ways for large-scale filtration of oil and water.[6] Their excellent processing features, such as recyclability of throughput material, ease of cleaning, and highly pure permeation attribute to their extensive use.[7] Among these, block copolymer (BCPs) membrane have been emerging as promising materials for fabrication of ultrafiltration membranes[8] due to several advantages including formation of various nanoscale morphologies, directed self-assembly for orientation control and selective etchability for nanochannel formation, potential to exhibit high uniformity pore size, and ultrahigh pore density.[9,10] Moreover, BCPs possess unique ability to self-assemble and form periodic microstructures[11] and tunable pore size (e.g. light driven shape-memory porous films with facile breath figure approach),[12] all essential characteristics for high flux and high selectivity performance criteria needed for industrial applications.[7] Zhou and Wang,[13] in a very recent study, addressed the selective swelling induced pore generation in polysulfone based BCP ultrafiltration membranes. Their “greener” melt extrusion-microwave boosted method was used for the pore generation, yet large scale production remains a challenge. Among the several BCP examples in the literature, Zhang et al.[14] made pH sensitive surfaces from poly(2-vinylpyridine-polydimethylsiloxane) membranes with switchable oil wettability (with change in media pH), and switchable acidic water wettability (various pH). However, the recovery of wettability and surface fabrication was complicated. Another study fabricated the fluorinated polyarylester-polydimethylsiloxane (PAR-b-PDMS) BCP from the monomers and used spray coating method

to develop superhydrophobic/superoleophilic porous BCP membranes[15]. Though the membrane achieved better mechanical properties and oil sorption performance, the complex BCP formation negated its cost-effectiveness.

In this work, we demonstrate the fabrication approach, characterization and testing of PS-b-PMMA BCP membranes by a dynamic thermal gradient annealing method developed by us, termed cold zone annealing (CZA)[16], followed by UV-processing for effective oil/water separation. The formation of vertically[17-20] oriented nanopores in the membranes is ensured by the CZA process followed by UV degradation of the PMMA cylindrical domains selectively into hydrophilic pores so that water molecules selectively pass through the membrane. Pronounced efficiency, comparatively less cost, and simplicity in design are considered as advantages of this method. Moreover, PS-b-PMMA is a widely available BCP intended to be a model membrane for oil/water separation applications.

Results and Discussion

The fabricated membranes consist of a supporting layer and a functional BCP thin film active "skin" layer with vertically oriented nanopores, as described in the experimental section. This is unlike previous BCP studies wherein the nanoporous channels are meandering in the thru-thickness direction providing for a more tortuous filtration path, resulting in higher filtration pressure requirements and lower throughput, compared to direct vertical nanopores reported here. The supporting layer for the BCP membrane was a commercial (BASF) microporous polyether-sulphone (PES) membrane. PES is a high temperature, acid- and base resistant polymer. The strength and durability of PES-based membrane filters is critical during the high pressure filtration procedures that require aggressive handling or automated equipment, Scheme 1 (SI). Figure 1 a) and 1 b) shows the surface morphology of the supporting macroporous PES membrane illustrating the generally uniform macropore dimensions. Figure 1 c) illustrates the optimum vertical order of CZA processed 100nm PS-PMMA film (bright spots are PMMA), by adjusting film thickness, CZA parameters of push speed, maximum temperature and temperature gradient, and Figure 1 d) shows the subsequent optimal etched pores film by adjusting UV and acetic acid etching conditions. Results of optimization of 1) of BCP film thickness, 2) varying CZA parameters of speed needed to fully control vertical orientation fraction, and 3) of subsequent chemical etching process to obtain clean, highest fraction of non-laterally connected etched pores, are briefly described next.

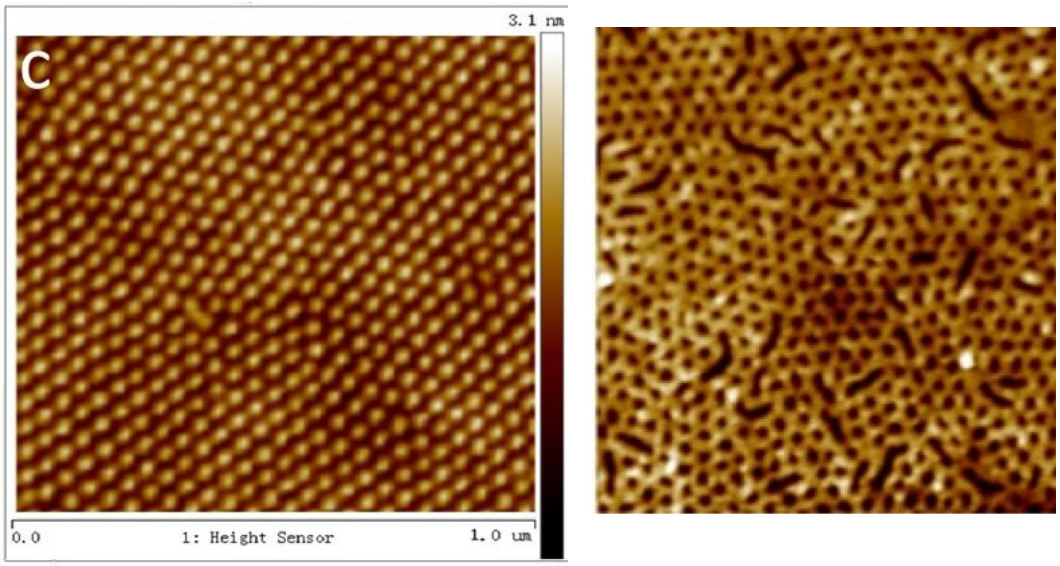

Figure 1 a.) SEM and b) AFM images of the top surface of the PES supporting membrane, and c) AFM image (1x1 μm^2) of surface morphology of a CZA annealed PS-b-PMMA film, prior to etching and d) after UV etch and acetic acid rinse.

Figure 2 illustrates the (low resolution) topographical morphologies for PS-b-PMMA thin functional layer with different thicknesses by flow coating prepared under the same CZA conditions. The vertically and parallel oriented cylinder ratios were analyzed using the software ImageJ. A strong dependence of the ratio of the BCP perpendicular cylinders orientation after annealing on the film thickness is evident. When the thickness increases from 70 nm to 100 nm, the ratio of the vertically oriented cylinders increases gradually from 37.2% to 94.3%, which indicates that 100 nm would be a desirable thickness for the membrane functional BCP layer. Films thicker than 100 nm exhibit lower vertical pore density due to a thickness dependent divergence of the thermal gradient at the film air surface, being imposed from the film bottom.

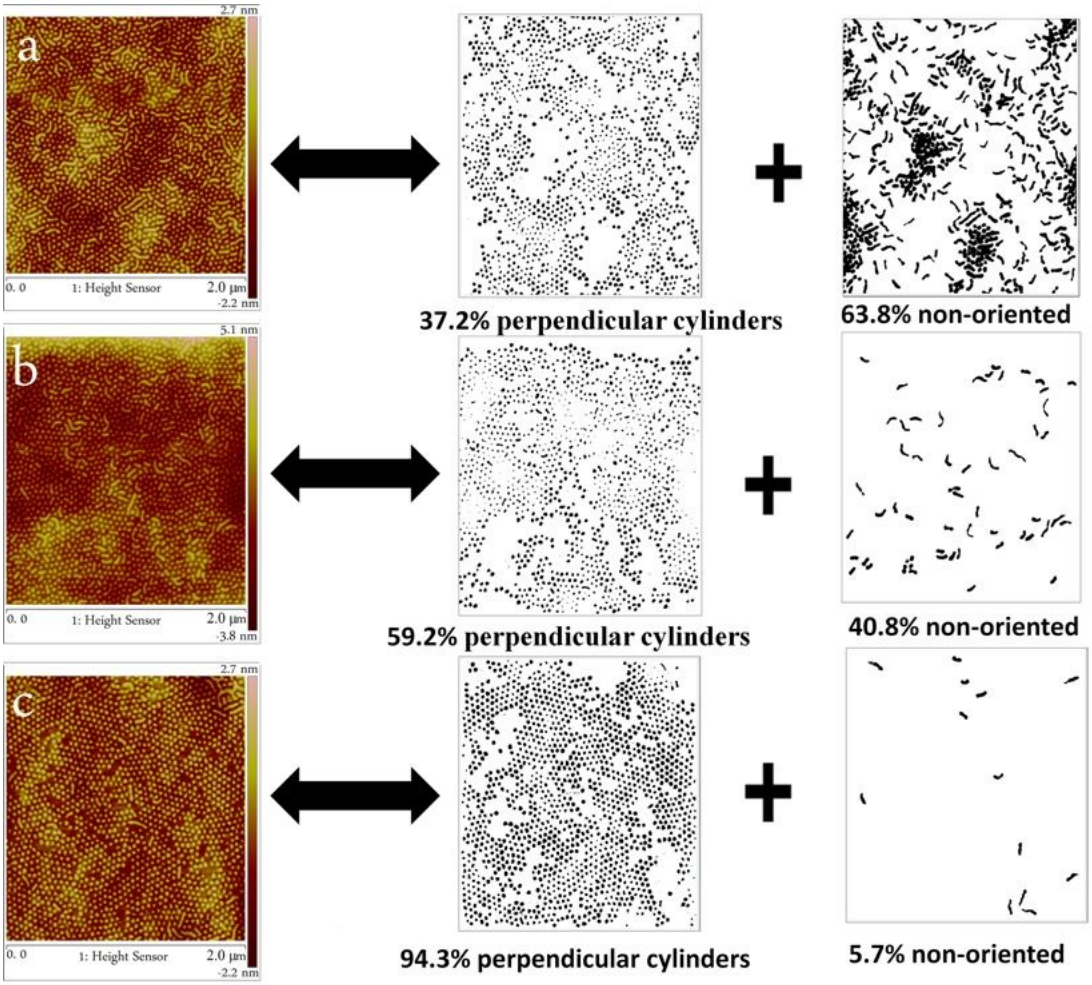

Figure 2. AFM images of CZA annealed BCP thin films with different thickness and their corresponding vertical and parallel cylinder percentage (see Experimental Section for vertical cylinder percentage calculation). Thicknesses and corresponding pore density: (a) 70 nm, 217.25/μm^2; (b) 85 nm, 317.97/μm^2; (c) 100 nm, 420.77/μm^2

The optimal thickness (~100 nm) to form vertically oriented cylinders is a trade-off between surface wetting forces for parallel orientation of PS and PMMA layers at air and substrate respectively, versus vertical driving forces via coupling of CZA dynamic rate (inverse CZA velocity) with the longest relaxation time of the BCP, reported previously by Singh et al.[17] Essentially, the in-plane thermal gradient of CZA induces vertical orientation and order simultaneously of the microphase of PS-b-PMMA[18-20] by transient thermal expansion forces coupled with inertial effects, while interfacial effects synergistically dominate ordering in thinner films from both air and substrate interfaces.

The CZA velocity (sweep rate) during the CZA process was found to have an important impact on the cylinder orientation of BCP thin films. Samples with the same thickness of 100 nm

were annealed using CZA at different sweep rates, and the corresponding AFM images are shown in Figure 3. Typical range of the sweep rate for vertical ordering is illustrated in Figure 3, a consequence of surface tension driven wettability kinetics versus polymer relaxation coupled to dynamic sweep rate. At relatively low sweep rates (<<5 μm/s, not shown), wetting of the block copolymers dominated by surface wetting morphology leads to a parallel ordering. At the same time, when the samples were annealed at relatively high sweep rates (>> 5 μm/s), there is not enough time for the block copolymers to relax under a sharp temperature gradient, and the ordering process is kinetically hindered. When the CZA sweep rate reaches ~10 μm/s, a well-ordered perpendicular cylinder morphology is obtained, albeit with limited fraction of parallel cylinders. Best case scenario was illustrated in Figure 1.

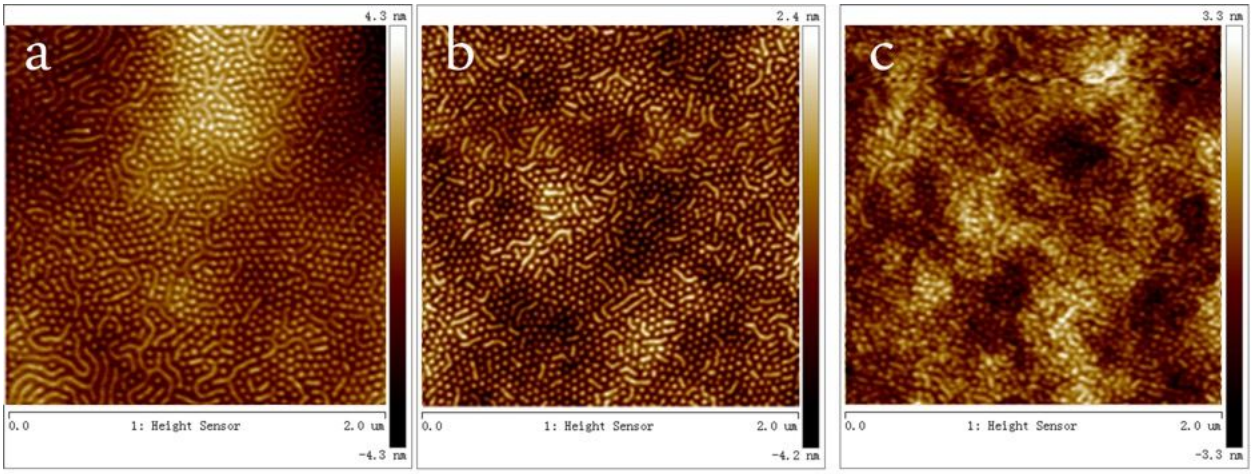

Figure 3. Typical AFM images of CZA annealed BCP thin films at different CZA sweep rate of 5 μm/s (a), 10 μm/s (b) and 15 μm/s (c). Image sizes are 2 μm x 2 μm

After the formation of perpendicular cylindrical morphology, PS-b-PMMA thin films were exposed to UV light under vacuum for different controlled exposure time, from 1h to 3h. The results of different UV exposure time, followed by rinsing with the solvent are shown in Figure 4, (a-e) and by TEM in Figure S1. With increasing UV exposure time, the cylinder-forming phase can be disintegrated. Specifically, after exceeding the exposure time above 1.5 hours, the PMMA phase was annihilated. Different volume fraction (25%, 50%, 75%, 100%) of acetic acid solution in distilled water was used for rinsing the thin films after etching. The results are shown in Figure 4 (f-i), indicate that the samples rinsed with 100% acetic acid corresponds to the best clarity of the images.

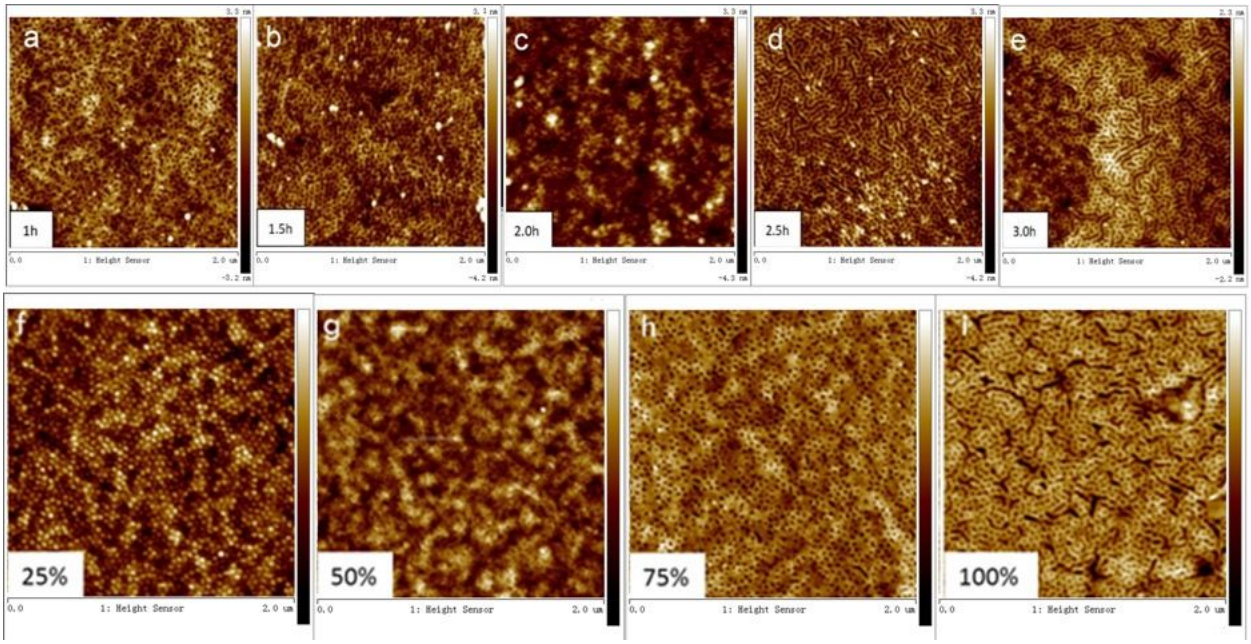

Figure 4. AFM images of identical CZA annealed PS-b-PMMA thin films under different ultraviolet etching time in absence of oxygen: (a) 1 hour; (b) 1.5 hours; (c) 2.0 hours; (d) 2.5 hours; (e) 3.0 hours. AFM images of CZA annealed, and UV etched PS-b-PMMA thin films washed with different concentration of acetic acid in distilled water: (f) 25% acetic acid in distilled water; (g) 50%; (h) 75%; (i) pure acetic acid.

From literature[21,22], the mechanism of acetic acid removal of UV degraded PMMA and revealed formation of (unspecified) oxide groups (increased O/C ratio by XPS). In general, UVO of polymers leads to atomic oxygen reaction with carbon chain through insertion or hydrogen abstraction reactions to produce oxidized entities such as carbonyl and carboxyl entities that are also hydrophilic.[23-26]

Membrane Filtration Tests. Preliminary demonstrative purposes membrane filtration tests were performed to demonstrate i) oil/water mixture separation and ii) polymer pore-size size based molecular weight filtration cut-off. Membrane pieces were cut to fit the dimensions to the Amicon 8010 stirred cell (Millipore Co., Cambridge, MA), Figure 5a and were secured afterward by a silicone O-ring. The stirred cell has an active working volume of 10 ml and a membrane area of 4.1 cm^2. A nitrogen cylinder provided the pressure, and a hot stage was used to elevate the temperature, as well as to provide a simultaneous stirring.

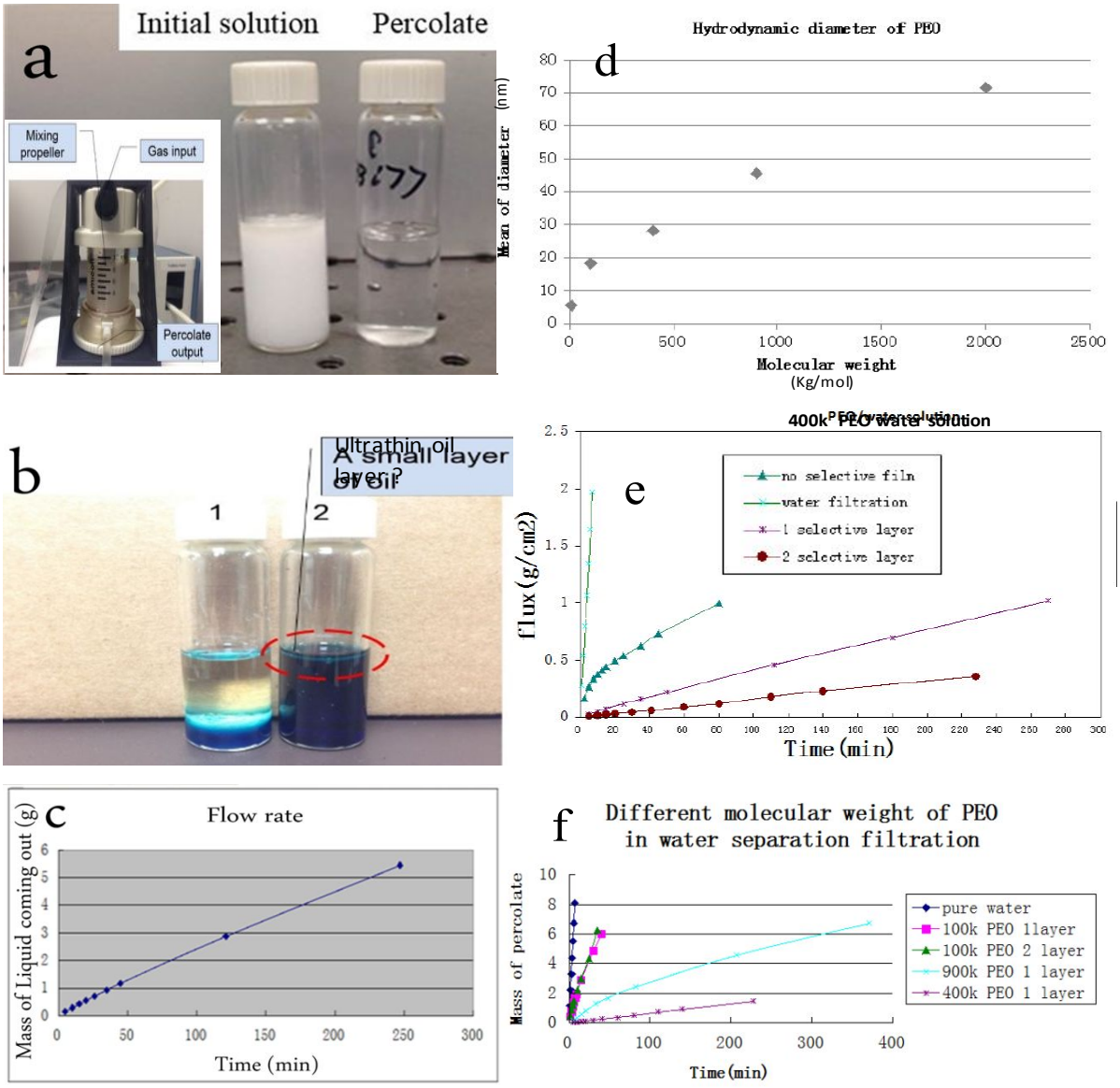

Figure 5. a) Comparison of the initial oil/water milky emulsion versus clear percolate (water) after filtration, showing the ultrafiltration pressure cell. b) Stained water/oil emulsion at quiescent bilayer state, and percolate solution after filtration c) The flow rate of oil/water emulsion under 10 psi and 200 rpm during filtration process. d) Hydrodynamic diameter (D_h) of PEO with different molecular weight by dynamic light scattering (5.44nm for 6.8k PEO, 18.20nm for 100k PEO, 28.18nm for 400k PEO, 45.60nm for 900k PEO, 71.54nm for 2000k PEO e) Flow rate of pure water, and 400k PEO/water solution through PES only, and using different configurations of 1-layer and 2-layer BCP membrane f) Flow rate (in g/cm^2) of different molecular weight PEO/water solution. A non-monotonic rate is observed with minima when PEO $D_h \sim$ 23 nm pore size.

i) Oil/water mixture separation: For demonstrating the oil/water emulsions separation properties of the etched BCP membrane, cooking (Canola) oil and water with the volume ratio of

1:1 was used for the initial composition. The permeation experiments were conducted at the stirring speed of 200 rpm and pressure of 10 psi, using the filtration cell shown in Figure 5a with milky oil/water emulsion and filtered clear water solution shown. Figure 5b, set up 1 shows settled bilayer of oil on blue dye labeled water. This is a vigorously shaken mixture prior to filtration. Set up 2 is the filtrated blue dye labeled liquid water (est ~99%), with potentially a trace of ultrathin layer of oil on top, however that may be a meniscus refractive index effect. Figure 5c shows that the throughput for the est. ~99% purity water flow, at the relatively low pressure of 10 psi (0.7 bar), is linear in time with the Flux ≈ 5.0 $l.m^{-2}.h^{-1}.bar^{-1}$. This is an acceptable rate in the range of water permeability of several RO/NF membranes[26], typically in the range of (1-10) $l.m^{-2}.h^{-1}.bar^{-1}$.

ii) Pore size limited polymer filtration: Characterization of the water flux rates and selectivity were performed using a series of poly (ethylene oxide) (PEO) solutions in water, with narrow molecular mass distribution, whose hydrodynamic diameter (D_h) ranging from ~ (5-72) nm were determined by dynamic light scattering (DLS) [9] as showing in Figure 5d and documented in Figure 5 caption. PEO concentrations of 1.5 g/L (below critical micelle concentration, CMC) were used at the stirring speed of 60 rpm at 10 psi pressure in the stirred cell module. The filtration efficiency was characterized by the ratio of the amounts of the polymer left after the evaporation, of filtrated to non-filtrated solutions. Figure 5e shows summary of various results for PEO with a molecular mass of 400 kg/mol and a hydrodynamic diameter of 28.2 nm dissolved in water. Figure 5 e shows highest flow rate occurs for pure water flow, followed by PEO/water solution, through a pure PES supporting membrane only as expected in filtration device. When the membrane was exposed only to water, the following equation[8] can be applied, $J=|\triangle P|/R_m\mu$. where ΔP is the pressure differential, R_m is the resistance to flow by the membrane, and μ is the chemical potential of the solvent. The next highest rate is for a single, "1-layer" etched BCP supported on PES membrane as expected. A CZA processed and etched PS-PMMA BCP membrane with a pore size of 23 nm was used for the filtration of the prepared solutions. After filtration, 1 μl of the percolate solution was put in the glass Petri dish and evaporated in a vacuum oven at 40 ℃. The weight of the remaining pure PEO was evaluated when the weight of the Petri dish became constant (~0.8 mg). By comparison, the weight of dried PEO was 1.5 mg for the initial non-filtrated solution after evaporation. This demonstrates a separation efficiency of the membrane of more than 50% for the 400k Mw PEO.

As the 100 nm BCP membrane fabrication process as illustrated in SI Scheme 1 is quite challenging in the absence of automation (success rate less than 50% when crafted by hand due to fragile nature of porous/etched BCP membrane), we explored the potential for fabricating more robust CZA-BCP-UVO membranes that are tolerant to defects (film crack, connected pore in UVO, wrinkle region) in individual layers. Thus, with multilayer in mind, we fabricated a 2-layer membrane by sandwiching a second supported layer membrane on top of an existing 1-layer membrane structure. Figure 5e clearly shows that with an increase of the number of the stacked selective layers from 1 to 2, the flow rate decreases ~ 50%, which indicates that there is a compromise between a better selectivity and a flux permeation rate. Notably, it is always required to place a PES supporting membrane on top of the membrane, not just as the bottom supporting layer, for mechanical integrity.

The flow rates for the PEO solutions of different molecular weights in water were measured as well (Figure 5f). Compared to the permeation process of pure water, the flow rate of PEO/water solutions was low as expected, that can be observed from the slopes of the curves (the slope for 100 K PEO is 0.0350 (g/cm^2)/min, 0.0016 (g/cm^2)/min for 400 K PEO, 0.0043 (g/cm^2)/min for 900 K PEO and 0.0035 (g/cm^2)/min for 2000 K PEO). Interestingly, for 400 K PEO, the flow rate has reached its lowest value of 0.0016 (g/cm^2)/min. We hypothesize that as the diameter of the 400 K PEO was around 28.2 nm, which is close to the pore size of the selective membrane of 23 nm, it tends to block the pores, resulting in lowest flow rate. With increase in the molecular mass of PEO to above 400 K, i.e. $D_h >> 23$ nm pore size, we hypothesize that the flow rate increases again due to the PEO chains passing through in an extensional "slinky" form of the chain. Since a 72 nm diameter PEO chain cannot pass through a 23nm BCP pore, this must be the molecular flow mechanism. As de Gennes predicted[27], the entropy of chain confirmation deformation is a low penalty for polymer chains in good solvents, so this is quite plausible. However further studies need to be done to confirm this phenomena.

In conclusion, a new nanoporous block copolymer membrane for oil/water separation has been introduced in this work. Cold zone annealing (CZA), a dynamic and roll-to-roll compatible method for continuous membrane production, and UV etching were used to fabricate the ultrafiltration membrane. This asymmetric membrane comprised of a 100 nm thick nanoporous selective thin film layer with monodisperse pores, that is tunable by molecular weight, and templated by block copolymer self-assembly. A conventional microfiltration PES membrane

forms the supporting layer. The paper explored the UV and acetic acid rinse etching conditions for optimal pore fidelity and formation density and multilayer fabrication. The membrane is demonstrated to work in preliminary oil/water separation experiments, and polymer separations from solution. The application of such block copolymer membranes provides a new paradigm and technique for ultrafiltration separation processes, with a potential for solving other filtration challenges involving application of membranes[28-30].

Conflicts of interest

There are no conflicts to declare.

Acknowledgements

This publication is made possible by NPRP grant 10-0127-170269 from the Qatar National Research Fund (a member of Qatar Foundation). The statements made herein are solely the responsibility of the authors.

References

[1] World Energy Outlook, **2014**. Organization for Economic Co-operation and Development (OECD)/International Energy Agency (IEA).

[2] Janson A, Minier-Matar J, Al-Shamari E, Hussain A, Sharma R, Rowley D, Adham S. Evaluation of new ion exchange resins for hardness removal from boiler feedwater. *Emergent Materials*. **2018**;*1(1-2)*:77-87.

[3] Parangusan H, Ponnamma D, Hassan MK, Adham S, Al-Maadeed MA. Designing carbon nanotube-based oil absorbing membranes from gamma irradiated and electrospun polystyrene nanocomposites. *Materials*. **2019**;*12(5)*:709.

[4] Ponnamma D, S Nair S, Parangusan H, K Hassan M, Adham S, Karim A, Al Ali Al-Maadeed M. White Graphene-Cobalt Oxide Hybrid Filler Reinforced Polystyrene Nanofibers for Selective Oil Absorption. *Polymers*. **2020**;*12(1)*:4.

[5] Essemiani K, Kroll S, Severing K, Kok JB. Pretreatment processes in a nutshell. *Hydrocarbon Engineering.* **2009***; 14*:76-84.

[6] Arun K. Kota, Gibum Kwon, Anish Tuteja. Hygro-responsive membranes for effective oil–water separation. *Nature Communications.* **2012** *August 28; 10:*1025-1038.

[7] Jackson AJ, Hilmyer MA. Nanoporous Membranes Derived from Block Copolymers: From Drug Delivery to Water Filtration. *ACS Nano 2010, 4, 7, 3548-3553*.

[8] Hayirlioglu A, Kulkarni M, Singh G, Al-Enizi AM, Zvonkina I, Karim A. Block copolymer ordering on elastomeric substrates of tunable surface energy. *Emergent Materials*. **2019**;*2(1)*:11-22

[9] Ahn H, Park S, Kim SW, Yoo P.J., Ryu DY, Russell. Nanoporous Block Copolymer Membranes for Ultrafiltration: A Simple Approach to Size Tunability. *ACS Nano* **2014**, 8 (11), 11745-11752.

[10] Tokarev, I.; Krenek, R.; Burkov, Y.; Schmeisser, D.; Sidorenko, A.; Minko, S.; Stamm, M., Microphase Separation in Thin Films of Poly(styrene-block-4-vinylpyridine) Copolymer-2-(4'-Hydroxybenzeneazo) benzoic Acid Assembly. *Macromolecules* **2005***, 38(2),* 507-516.

[11] Phillip WA, O'Neill B, Rodwogin M, Hillmyer MA, Cussler EL. Self-assembled block copolymer thin films as water filtration membranes. *ACS applied materials & interfaces.* **2010** *March; 2(3):*847-53.

[12] Wang W, Shen D, Li X, Yao Y, Lin J, Wang A, Yu J, Wang ZL, Hong SW, Lin Z, Lin S. Light driven shape memory porous films with precisely controlled dimensions. *Angewandte Chemie International Edition*. **2018**; *57(8)*: 2139-43.

[13] Zhou, J. and Wang, Y., Selective Swelling of Block Copolymers: An Upscalable Greener Process to Ultrafiltration Membranes?. *Macromolecules*, 2020, 53, 1, 5–17.

[14] Zhang L, Zhang Z, Wang P. Smart surfaces with switchable superoleophilicity and superoleophobicity in aqueous media: toward controllable oil/water separation. *NPG Asia Materials*. **2012**;*4(2)*:e8-.

[15] Li H, Zhao X, Wu P, Zhang S, Geng B. Facile preparation of superhydrophobic and superoleophilic porous polymer membranes for oil/water separation from a polyarylester polydimethylsiloxane block copolymer. *Journal of materials science*. **2016**;*51(6)*:3211-8.

[16] Berry, B., Bosse, A., Douglas, J.F., Jones, R.L., Karim, A., Orientational Order in Block Copolymer Films Zone Annealed below the Order−Disorder Transition Temperature. *Nano Lett. 2007, 7, 9, 2789–2794*.

[17] Singh, G., Yager, K.G., Smilgies, D.M., Kulkarni, M.M., Bucknall, D.G. and Karim, A., Tuning molecular relaxation for vertical orientation in cylindrical block copolymer films via sharp dynamic zone annealing. *Macromolecules*, **2012**. *45*(17), pp.7107-7117.

[18] Singh, G., Yager, K., Berry, B., Karim, A., Dynamic thermal field-induced gradient soft-shear for highly oriented block copolymer thin films. *ACS Nano.* **2012***; 6(11):*10335-10342.

[19] Singh, G., Batra, S., Zhang, R., Yuan, H., Yager, K.G., Cakmak, M., Berry, B., Karim, A., Large-Scale Roll-to-Roll Fabrication of Vertically Oriented Block Copolymer Thin Films, *ACS Nano*. **2013**, 7, 6, 5291–5299

[20] Basutkar, M.N., Samant, S., Strzalka, J., Yager, K.G., Singh, G., Karim, A. Through-Thickness Vertically Ordered Lamellar Block Copolymer Thin Films on Unmodified Quartz with Cold Zone Annealing. *Nano Lett.* **2017**. 17(12):7814 - 7823.

[21] Freychet, G., Maret, M., Tiron, R., Chevalier, X., Gharbi, A., Fernandez R.M., Gergaud, P., Removal of poly(methyl methacrylate) in diblock copolymers films studied by grazing incidence small-angle X-ray scattering, *Journal of Polymer Science, Part B: Polymer Physics*, (2016) 54(12), pp. 1137-1144.

[22] Lin, T.Y., Pfeiffer, T.T., Lillehoj, P.B., Stability of UV/ozone-treated thermoplastics under different storage conditions for microfluidic analytical devices, *RSC Adv.* (2017) 7(59): 37374–37379.

[23] Time-of-flight Secondary Ion Mass Spectrometry (TOF-SIMS) for high-throughput characterization of Biosurfaces, Robertson, S., Sehgal, A., Fahey, A., Karim, A., *Applied Surface Science*, (2003) 203-204 pp. 855-858.

[24] Teare, D.O.H., Ton-That, C., Bradley, R.H., Surface characterization and aging of ultra-violet-ozone treated polymers using atomic force microscopy and x-ray photoelectron spectroscopy, *Surf. Interf. Anal.,* (2000) 29, pp. 276-283.

[25] Ye, T., Wynn, D., Dudek, R., Borguet, E., Photoreactivity of alkylsiloxane self-assembled monolayers on silicon oxide surfaces, *Langmuir* (2001) 17, pp. 4497-4500.

[26] Ochando-Pulido, J.M., Martínez-Férez, A., Stoller, M., Analysis of the Flux Performance of Different RO/NF Membranes in the Treatment of Agroindustrial Wastewater by Means of the Boundary Flux Theory, *Membranes* (2019) 9, 2.

[27] de Gennes, P.G., *Scaling Concepts in Polymer Physics,* Cornell University Press, 1979.

[28] Kennedy, K.E., Shafique, N., Douglas, J.F., Starr, F.W.. Cooperative dynamics in a model DPPC membrane arise from membrane layer interactions, *Emergent Mater.* 2, 1–10 (2019).

[29] Shah, S., Shah, M., Shah, A., Shah, M., Evolution in the membrane-based materials and comprehensive review on carbon capture and storage in industries, *Emergent Mater.* (2020) 3, 33–44.

[30] Esteves, R.J.A., Gornick, V., Alqurwani, D.S. et al. Activated carbon-doped polystyrene fibers for direct contact membrane desalination, *Emergent Mater.* (2020) 25 May 2020 https://doi.org/10.1007/s42247-020-00107-z